

We are IntechOpen, the world's leading publisher of Open Access books Built by scientists, for scientists

6,900

Open access books available

185,000

International authors and editors

200M

Downloads

Our authors are among the

154

Countries delivered to

TOP 1%

most cited scientists

12.2%

Contributors from top 500 universities



WEB OF SCIENCE™

Selection of our books indexed in the Book Citation Index
in Web of Science™ Core Collection (BKCI)

Interested in publishing with us?
Contact book.department@intechopen.com

Numbers displayed above are based on latest data collected.
For more information visit www.intechopen.com



Exploration for Fe-Mn Oxides Using Geochemical Signatures in Soil: A Case Study of Part of Northwestern Nigeria

Olufemi Sijuade Bamigboye

Abstract

Part of northwestern Nigeria was investigated with the aim of delineating concealed mineralization using geochemical signatures in soils. To achieve this, 30 selected soil samples were analysed geochemically. The result of the elemental analysis was subjected to Principal Component Analysis (PCA) and isograde plotting, while selected elements were correlated. From the geochemical result, most of the analysed elements have anomalous value in the southern part of the area, while the least values are in the southwestern. From the PCA analysis, six factor groups were distinct. The factor groups were interpreted geochemical to fingerprint mineralization in the area. The result of correlation analysis shows that Fe is negatively correlated with most of the correlated elements. The study concluded that the central part of the study area is mineralized with both manganite and goethite. In addition, manganese mineralization is indicated by elemental association: Zn+As+Be+Bi+Co+Nb+Ni+CsP+Al+Ca+Cd+Li+K, while iron mineralization is indicated with Zr+Th+Pd+Mo+V+Sn+Cr+Ce+InSc+P+Pb association.

Keywords: manganite, goethite, Kaoje, exploration geochemistry, soil survey

1. Introduction

Traditional exploration geochemistry usually employs earth materials such as rock, stream sediment and soil to detect unusual concentration of elements that may serve as pathfinder for concealed ore body [1–3]. The distribution of pathfinder elements in these media especially stream sediment and soil is governed by weathering and hydromorphic conditions of the area under investigation in addition to the mobility of such elements. Despite their dispersion, trace and rare earth elements still retain their bedrock characteristics. These elements are adsorbed unto surfaces of weathered products and possess the ability to remain on the surfaces of these weathered particles for long periods unless they are mobilized by decomposition processes such as redox conditions [4]. Bowen [5] believes that the residence time of these elements in temperate soils is not the same. For example, the residence time of Pb is between 740 and 5900 years, Zn has a residence time of 70–510 years, 13–1100 years is the residence time for Cd, and 310–1500 years is the residence time for Cu, while the residence time in tropical soils is 40 years due to the shorter rate of

leaching. Soil geochemical surveys have proven to be highly effective with long and impressive history of discovering blind deposits [6].

Akilolu [7] reports the gossan manganite occurrences in Buya and Derena area, northwestern Nigeria. He groups these ores into three which are Buya, Derena north and Derena south clusters. In his paper, he argues that the Buya gossans are purer than other clusters. Bamigboye et al. [8] report goethite mineralization in addition to the manganite mineralizations reported by Akilolu [7] in Kaoje, northwestern Nigeria. Furthermore, an exposure of brown laminated manganite ore, south of Barkin-Ruwa, was also reported to earlier reported manganite clusters in these areas. This exposure is relatively unique in terms of its brown colouration as against the black colour of those in Buya and Derena clusters. The report of Akilolu [7] and Bamigboye et al. [8] did, however, not give account of the distribution of trace and rare earth elements in the soil in Kaoje and its environs, neither is vivid account given on the possibility of discovering concealed bodies of these ores or others within Kaoje and its environs. Other work related to this include the work of Adekoya [9], Mucke [10], Okorie et al. [11, 12] and Fillie [13, 14], among others. This work is therefore aimed at identifying the mineralized zones in Kaoje and its environs using geochemical signatures in soils around Kaoje and its environs, northwestern Nigeria. The study area is bounded by Long. 3°55' and 4°10'E and Lat. 11°00' and 11°15'N covering an approximate area of 676 km².

2. Geology of the study area

The geology of the area can grossly be divided into the basement complex rock and sedimentary rocks. The basement complex rocks are mainly banded gneiss, migmatite, granite gneiss, quartz-mica schist and granite (**Figure 1**).

The banded gneiss occurs as elongated rock body within the schist and is seen about 2 km south-west of Buya and midway between Idowa and Derena. The banded gneisses are rich in quartz with pervasive jointing, filled by quartz and quartzofeldspathic vein in most cases. Migmatite trends in SE-NW direction mainly. The granite gneisses have a sharp contact with the mica schist. Mineralogically, quartz, biotite and sodic feldspar predominate, but crystals of tourmaline are seen in some localities. The quartz-mica schist is extensively weathered and covers about one-fifth of the area studied. It occurs as a low-lying exposure and stream-cut exposure. Some of the schists occur as xenolith with a large pegmatitic body close to Barkin-Ruwa, along Barkin-Ruwa-Buya road.

The granitic bodies occur towards the southern part of the study area. The granitic rocks occur as boulders and cobbles of rocks and are closely associated with weathered schist in the southernmost part of the area. The pegmatitic rocks in this area are seen associated with the schist and migmatite mainly. Some of the pegmatites are also seen at the contact between the schist and the sedimentary rock in the northwestern area. Mineralogically, the pegmatites are made up of quartz, biotite, k-feldspar tourmaline (in the southeastern part) and chalcedony (in the northwestern part).

Sedimentary rocks in this area occupy about 60% of the area. This rock includes the Biongba, Morongba and Koremi hills. These hills are essentially clastic sedimentary rocks that include the sandstone and silty sandstone. In the northeastern part of Kaoje, sedimentary rocks occur as remnant of gully eroded sedimentary rocks. These rocks are finely laminated with characteristic ichnofossil. Other characteristic of these rocks are their semi-consolidated nature that is typical of Taloka Formation in the Sokoto Basin. The rocks in this area include silty sandstones that are finely laminated, while some are massive. Other sedimentary rock types seen associated with the sandstone are goethite, kaolinitic mudstone, finely laminated

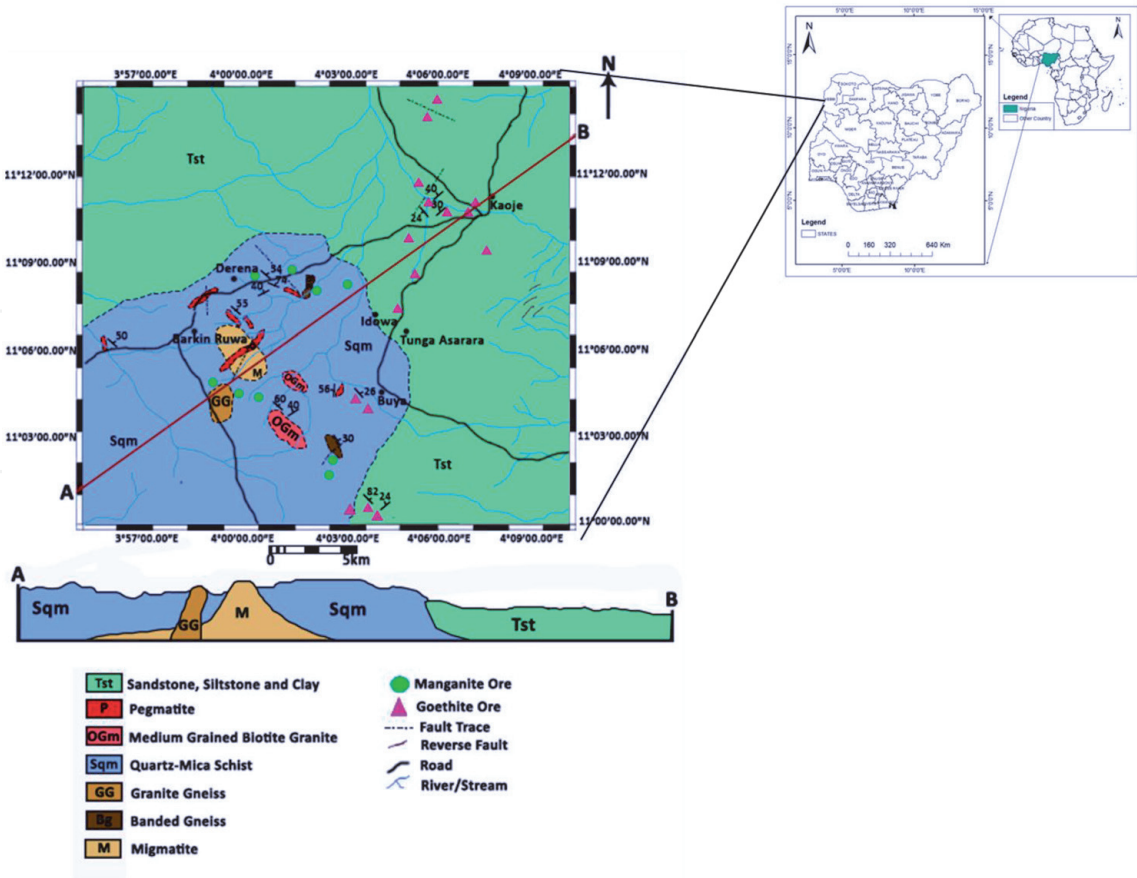


Figure 1.
Geological map of Kaoje and its environs with inset of map of Nigeria and Africa.

siltstones and kaolinitic purple claystone. All these are exposed along Kaoje-Idowa road and towards the edge of the area studied in the northeastern part.

The iron ore occur as vein, boulders and sedimentary capping in the northeast and southeast mainly. It shows conspicuous alternating bands of iron and chert-rich layers in most of the location, while few are massive iron ore with little or no cherty contents. Bamigboye et al. [8] describe these irons to be of hydrothermal origin but now remobilized. Manganite gossans occur as boudins in an almost NE-SW direction from Buya through Derena to the eastern part of Barkin-Ruwa. These ores occur as black laminated exposures mainly around the Buya-Derena axis and as brown folded brown laminated body south of Barkin-Ruwa. Mn is associated with quartz veins. From the work of Bamigboye et al. [8], the iron ores are made up of feroxhyte, gibbsite, goethite, maghemite, magnetite and haematite essentially with subordinate manganite, while the manganites are composed of manganite, gibbsite, magnetite, bayerite, akaganeite and nordstrandite among others.

3. Methodology

The methods adopted in this work are grossly divided into two. These are fieldwork and laboratory work. The fieldwork was carried out between 2011 and 2012. During this period, rock and soil samples were taken. The soil samples were taken from a grid of 1 km × 1 km from a depth range of 30–50 cm corresponding to the B-horizon as recommended by Vareikiene and Lehtonen [15]. Thirty soil samples were prepared and subjected to geochemical analysis at ACME Analytical laboratory, Vancouver, Canada. In the laboratory, 0.5 g of the soil samples were

digested with a modified aqua regia solution of equal parts concentrated HCl, HNO₃ and DI H₂O for 1 h in a heating block. The resulting solution was thereafter analysed by ICP-ES and ICP-MS for trace and rare earth elemental concentration. The selected elements that were considered related to iron and manganite mineralization from the geochemical data was correlated. Others were subjected to principal component statistical analysis (PCSA) using the SPSS software, while isograde plotting of the data was done using Surfer 12.

4. Results and interpretation

The result of the geochemical analysis where the concentration of 53 elements was determined is shown in **Table 1**. From the result, sample 83a and 86 had the highest concentration of most of the elements, while sample 64 and 222 had the lowest concentration of most of the elements. S had a constant value of <0.02 except in sample 83a where the value is 0.02%. This same sample had 0.05 ppm concentration of W as against <0.05 in the remaining samples. This is equally similar to the slight higher concentration of 0.02 ppm concentration of Se as against <0.1 in other samples.

The good correlation coefficient of Mn with Ni and Mg and the weak correlation especially between Mn and Cu are related to Mn-rich end member (**Table 2**). Similarly, good correlation coefficients between Fe and Ti and P coupled with the correlation between Co and Ti and the weak-to-low correlation between Ti and Ca, Ca and P, Ca and Co, and Ca and Fe are all related to Fe-rich end member. Likewise, the strong correlation between Al and K ($r = 0.845$) is related to aluminosilicate minerals, while the fairly good correlation coefficients between Mg and Mn and Cr and Ca are related to mantle-derived ultramafic materials.

The result of the PCA shows a total of six factor groups (**Table 3** and **Figure 2**). These are factors 1–6. Factor 1 with Mg, Ni, Cs, K, Te, Li, Ti, Rb, Bi, Al, Zn, Cu, Tl, U, Cr, Co, Na and Be accounts for a total of 43.59% before rotation and 31.86% after rotation. This is factor 2 with Zr, Hf, Th, Ga, In, Sc, Sn, Fe, V, Pd, Mo, Sb and As, and Ce accounts for 20.701% before rotation and 23.09% after rotation. Factor 3 has Se, Nb, Ca, Sr and P. This factor group accounts for 9.95% before rotation and 14.697% after rotation. Factor 4 with Ba, Pb, Y, Mn, La and Cd gave an account of 8.518% before rotation and 10.078% after rotation, while factor 5 with the following elements: Hg, Ag and Au account for 3.412% before rotation and 2.758% after rotation. Factor 6 does not have the highest loading of any element. Despite this, it still accounts for 2.658% before rotation and 3.106% after rotation.

Factor 1 of the principal component analysis of the soil was related to the weathering of the hydrothermal sulphide ore and silicate-rich banded iron formation [16, 17], while factor 2 was the product of weathered chert-rich magnetite and ores that are rich in terrigenous materials. The inclusion of elements, like Sn and Mo, indicates weathering of granitic rocks like pegmatite that had protore of some sulphide minerals [18]. The presence of Pd, Ce and Sb in this factor group attested to the presence of these minerals [16].

Factor 3 was related to the rocks and minerals such as phosphate REE-Nb deposits in an evaporite environment, while factor 4 was interpreted as the product of weathered manganese ore. Factor 5 was related to the weathered precious metals that were originally formed from hydrothermal sulphide ore [18]. Factor 6 had the second loading value of Mn, Sb and Co. This factor though not having the highest loading factor of any of the elements showed the weathering of Co-bearing manganese ore [19] and incompleteness or leakages in the system. These leakages typified by factor 6 were pronounced by the mobility of some of the elements. Factors 1–5

Sample no.	Cd (ppm)	Sb (ppm)	Bi (ppm)	V (ppm)	Ca (%)	P (%)	La (ppm)	Cr (ppm)	Mg (%)	Ba (ppm)	Ti (%)	B (ppm)	Al (%)	Na (%)	K (%)	W (ppm)	Sc (ppm)	Tl (ppm)	S (%)	Hg (ppb)
10	<0.01	0.04	0.06	17	0.02	0.006	9.4	9.0	0.02	18.7	0.009	<20	0.43	<0.001	0.03	<0.05	2.3	0.05	<0.02	11
18	0.02	0.05	0.05	22	0.15	0.009	15.8	15.1	0.03	42.4	0.019	<20	0.41	<0.001	0.03	<0.05	2.4	0.04	<0.02	30
33	<0.01	0.04	0.05	14	0.02	0.004	8.9	11.3	0.02	14.5	0.021	<20	0.23	<0.001	0.01	<0.05	1.6	0.03	<0.02	6
44	<0.01	<0.02	0.11	20	0.03	0.006	12.4	12.5	0.07	40.3	0.018	<20	0.45	0.002	0.08	<0.05	2.1	0.11	<0.02	9
60	<0.01	0.06	0.07	45	0.08	0.011	13.4	20.8	0.03	50.8	0.008	<20	0.49	<0.001	0.03	<0.05	2.3	0.07	<0.02	14
64	<0.01	<0.02	0.02	10	0.03	0.004	7.1	6.0	0.02	42.4	0.004	<20	0.14	<0.001	0.02	<0.05	1.0	0.03	<0.02	8
73	<0.01	0.02	0.04	13	0.03	0.005	7.3	8.1	0.02	33.4	0.008	<20	0.25	<0.001	0.02	<0.05	1.3	0.04	<0.02	7
76	0.01	0.03	0.05	33	0.01	0.010	10.9	21.3	0.02	15.1	0.014	<20	0.69	<0.001	0.01	<0.05	5.2	0.04	<0.02	14
78	<0.01	0.03	0.05	21	0.06	0.008	16.1	14.2	0.02	19.1	0.012	<20	0.47	<0.001	0.02	<0.05	2.7	0.03	<0.02	19
83a	0.02	<0.02	0.15	19	0.74	0.020	24.4	10.7	0.24	135.9	0.068	<20	1.55	0.003	0.42	0.05	2.0	0.33	0.02	17
86	0.01	<0.02	0.22	59	0.13	0.011	24.2	44.8	0.50	144.3	0.096	<20	1.98	0.003	0.51	<0.05	6.9	0.29	<0.02	11
112	<0.01	0.05	0.05	26	0.05	0.008	14.8	17.5	0.02	26.5	0.023	<20	0.38	<0.001	0.02	<0.05	3.2	0.04	<0.02	23
122	<0.01	0.07	0.11	73	<0.01	0.010	21.0	24.7	0.01	9.1	0.024	<20	1.07	<0.001	0.02	<0.05	7.8	0.07	<0.02	23
128	<0.01	0.04	0.05	45	0.07	0.011	14.1	21.2	0.02	45.0	0.015	<20	0.55	<0.001	0.03	<0.05	3.4	0.03	<0.02	15
135	<0.01	0.05	0.09	39	0.02	0.008	15.4	19.1	0.03	14.6	0.022	<20	0.74	<0.001	0.03	<0.05	5.4	0.06	<0.02	15
151	0.01	0.04	0.06	25	0.14	0.009	17.4	11.2	0.04	86.3	0.009	<20	0.42	<0.001	0.05	<0.05	2.4	0.06	<0.02	28
187	0.02	0.04	0.03	18	0.05	0.006	12.5	14.3	0.02	30.8	0.019	<20	0.25	<0.001	0.02	<0.05	2.1	0.03	<0.02	34
190	<0.01	0.04	0.05	23	0.03	0.007	12.2	17.0	0.02	18.7	0.027	<20	0.44	<0.001	0.02	<0.05	3.0	0.04	<0.02	28
194	<0.01	0.05	0.08	43	<0.01	0.011	11.0	19.6	0.01	7.4	0.013	<20	0.87	<0.001	0.02	<0.05	5.3	0.05	<0.02	16
199	<0.01	0.05	0.06	24	0.11	0.011	17.8	18.8	0.03	17.4	0.024	<20	0.46	<0.001	0.04	<0.05	3.0	0.05	<0.02	29
214	<0.01	<0.02	0.06	17	0.26	0.007	20.0	9.5	0.11	154.3	0.009	<20	0.53	0.001	0.08	<0.05	3.1	0.10	<0.02	22
217a	<0.01	<0.02	0.04	14	0.09	0.006	14.4	10.1	0.04	40.0	0.005	<20	0.38	<0.001	0.03	<0.05	1.7	0.05	<0.02	21

Sample no.	Cd (ppm)	Sb (ppm)	Bi (ppm)	V (ppm)	Ca (%)	P (%)	La (ppm)	Cr (ppm)	Mg (%)	Ba (ppm)	Ti (%)	B (ppm)	Al (%)	Na (%)	K (%)	W (ppm)	Sc (ppm)	Tl (ppm)	S (%)	Hg (ppb)
219	0.02	0.05	0.07	40	0.15	0.010	21.6	13.9	0.06	259.8	0.012	<20	0.46	0.003	0.03	<0.05	2.9	0.16	<0.02	13
222	<0.01	<0.02	0.02	6	0.04	0.003	8.5	5.8	0.02	28.8	0.005	<20	0.17	0.002	0.02	<0.05	1.5	0.03	<0.02	8
225	<0.01	<0.02	0.08	24	0.11	0.007	17.3	15.2	0.08	59.2	0.004	<20	0.76	<0.001	0.07	<0.05	3.7	0.13	<0.02	13
244	<0.01	0.05	0.07	36	0.04	0.011	14.9	14.9	0.03	27.4	0.025	<20	0.56	0.001	0.03	<0.05	3.5	0.06	<0.02	20
258	0.02	0.03	0.06	18	0.11	0.010	24.5	10.8	0.07	190.6	0.008	<20	0.43	0.001	0.06	<0.05	2.6	0.06	<0.02	27
261	0.02	0.04	0.07	29	0.09	0.009	22.9	11.6	0.04	68.9	0.010	<20	0.47	<0.001	0.04	<0.05	2.9	0.06	<0.02	25
266	0.02	0.05	0.07	30	0.08	0.013	30.6	15.6	0.04	43.8	0.021	<20	0.48	<0.001	0.04	<0.05	3.7	0.07	<0.02	29
286	0.01	0.04	0.09	42	0.06	0.009	18.3	12.6	0.03	43.9	0.011	<20	0.82	<0.001	0.04	<0.05	4.7	0.08	<0.02	21
Sample no.	Se (ppm)	Te (ppm)	Ga (ppm)	Cs (ppm)	Ge (ppm)	Hf (ppm)	Nb (ppm)	Rb (ppm)	Sn (ppm)	Ta (ppm)	Zr (ppm)	Y (ppm)	Ce (ppm)	In (ppm)	In (ppm)	Re (ppb)	Be (ppm)	Li (ppm)	Pd (ppb)	Pt (ppb)
10	<0.1	<0.02	2.6	0.48	<0.1	<0.02	0.15	8.7	0.5	<0.05	1.4	8.11	33.8	0.03	0.03	<1	0.3	1.2	<10	<2
18	<0.1	<0.02	3.1	0.36	<0.1	0.09	0.65	7.4	0.7	<0.05	3.2	9.57	33.1	0.02	0.02	<1	0.2	1.2	<10	<2
33	<0.1	<0.02	2.1	0.28	<0.1	0.07	0.37	4.7	0.6	<0.05	2.8	5.35	21.8	<0.02	<0.02	<1	0.1	0.7	<10	<2
44	<0.1	<0.02	2.7	1.16	<0.1	<0.02	0.18	17.9	0.5	<0.05	0.9	5.62	25.8	0.02	0.02	<1	0.4	3.4	<10	<2
60	<0.1	<0.02	3.1	0.39	<0.1	0.04	0.26	8.9	0.5	<0.05	2.3	8.98	33.2	<0.02	<0.02	<1	0.5	1.1	<10	<2
64	<0.1	<0.02	0.8	0.22	<0.1	<0.02	0.10	3.9	0.2	<0.05	0.6	3.85	12.7	<0.02	<0.02	<1	0.1	0.6	<10	<2
73	<0.1	<0.02	1.7	0.26	<0.1	<0.02	0.17	5.1	0.3	<0.05	1.1	4.63	21.8	<0.02	<0.02	<1	0.3	0.6	<10	<2
76	<0.1	<0.02	5.5	0.44	<0.1	0.17	0.35	2.8	0.9	<0.05	8.7	9.11	35.2	0.04	0.04	<1	0.2	1.0	<10	<2
78	<0.1	<0.02	3.0	0.42	<0.1	0.03	0.33	5.4	0.6	<0.05	1.9	10.48	55.0	<0.02	<0.02	<1	0.2	1.1	<10	<2
83a	0.2	<0.02	7.2	3.66	<0.1	0.11	2.63	57.1	1.1	<0.05	3.8	4.52	49.0	<0.02	<0.02	<1	1.4	28.8	<10	<2
86	<0.1	0.05	7.5	4.66	<0.1	0.03	0.49	55.1	1.0	<0.05	1.7	10.84	60.8	0.03	0.03	<1	1.1	32.2	<10	<2
112	<0.1	<0.02	3.5	0.41	<0.1	0.04	0.50	7.1	0.8	<0.05	3.3	9.72	41.0	0.03	0.03	<1	0.3	0.9	<10	<2

Sample no.	Se (ppm)	Te (ppm)	Ga (ppm)	Cs (ppm)	Ge (ppm)	Hf (ppm)	Nb (ppm)	Rb (ppm)	Sn (ppm)	Ta (ppm)	Zr (ppm)	Y (ppm)	Ce (ppm)	In (ppm)	In (ppm)	Re (ppb)	Be (ppm)	Li (ppm)	Pd (ppb)	Pt (ppb)
122	<0.1	<0.02	9.5	0.81	<0.1	0.36	0.35	5.5	1.6	<0.05	19.6	10.67	79.6	0.05	0.05	<1	0.2	1.4	14	<2
128	<0.1	<0.02	4.5	0.41	<0.1	0.05	0.45	6.0	0.9	<0.05	2.4	11.38	38.4	<0.02	<0.02	<1	0.3	1.1	<10	<2
135	<0.1	<0.02	7.0	0.75	<0.1	0.22	0.25	10.8	1.3	<0.05	11.2	9.41	85.1	0.04	0.04	<1	0.3	1.7	<10	<2
151	<0.1	<0.02	2.3	0.39	<0.1	0.06	0.26	9.9	0.4	<0.05	2.4	13.53	47.9	0.02	0.02	<1	0.4	1.2	<10	<2
187	<0.1	<0.02	2.0	0.29	<0.1	0.05	0.40	5.4	0.7	<0.05	2.9	9.95	26.0	<0.02	<0.02	<1	0.2	0.7	<10	<2
190	<0.1	<0.02	3.9	0.42	<0.1	0.04	0.39	6.5	0.8	<0.05	3.9	8.94	40.4	0.03	0.03	<1	0.2	1.2	<10	<2
194	<0.1	<0.02	6.8	0.55	<0.1	0.19	0.43	5.0	1.4	<0.05	10.5	5.06	48.3	0.04	0.04	<1	0.2	1.5	<10	<2
199	<0.1	<0.02	4.1	0.41	<0.1	0.08	0.54	7.9	1.0	<0.05	3.4	10.10	45.8	<0.02	<0.02	<1	0.3	1.1	<10	<2
214	<0.1	<0.02	2.3	0.46	<0.1	0.04	0.25	14.1	0.7	<0.05	2.1	15.96	43.3	<0.02	<0.02	<1	1.0	3.1	<10	<2
217a	<0.1	0.02	1.6	0.32	<0.1	<0.02	0.13	8.0	0.3	<0.05	1.1	8.44	31.5	<0.02	<0.02	<1	0.3	1.1	<10	<2
219	<0.1	<0.02	3.1	0.50	<0.1	0.07	0.40	8.2	0.6	<0.05	3.6	17.46	78.6	0.02	0.02	<1	0.6	1.2	<10	<2
222	<0.1	<0.02	0.9	0.26	<0.1	<0.02	0.09	4.0	0.2	<0.05	0.4	4.74	17.6	<0.02	<0.02	<1	0.4	0.6	<10	<2
225	<0.1	<0.02	4.1	0.82	<0.1	0.04	0.18	14.3	0.6	<0.05	2.0	9.58	39.4	<0.02	<0.02	<1	0.7	3.1	<10	<2
244	<0.1	0.03	4.5	0.56	<0.1	0.07	0.48	9.8	1.1	<0.05	4.4	10.24	54.8	<0.02	<0.02	<1	0.4	1.5	<10	<2
258	<0.1	<0.02	1.9	0.44	<0.1	0.03	0.26	11.2	0.4	<0.05	1.1	24.93	48.4	<0.02	<0.02	<1	0.7	1.3	<10	<2
261	<0.1	<0.02	3.5	0.57	<0.1	0.06	0.25	8.9	0.8	<0.05	3.3	14.57	83.8	<0.02	<0.02	<1	0.4	1.4	<10	<2
266	<0.1	<0.02	3.7	0.66	<0.1	0.04	0.53	12.4	1.2	<0.05	3.1	22.52	58.9	<0.02	<0.02	<1	0.4	1.8	<10	<2
286	<0.1	<0.02	6.0	0.82	<0.1	0.15	0.35	10.8	1.0	<0.05	7.6	15.61	45.8	0.04	0.04	<1	0.4	2.1	<10	<2

Table 1.
Geochemical result of the analysis soil samples.

	Mo	Pb	Zn	Ni	Co	Mn	Fe	As	Th	Sr	Cd	Bi	V	Ca	P	Cr	Mg	Al	K	Sc	Cs	Nb	Rb	Sn	Zr	Ce	In	Be	Li	Pd
Mo	1																													
Pb	0.610	1																												
Zn	0.499	0.332	1																											
Ni	0.674	0.412	0.767	1																										
Co	0.523	0.602	0.525	0.752	1																									
Mn	0.374	0.593	0.439	0.615	0.924	1																								
Fe	0.930	0.667	0.482	0.521	0.388	0.267	1																							
As	0.827	0.506	0.693	0.605	0.352	0.240	0.854	1																						
Th	0.634	0.564	0.091	0.090	0.043	−0.050	0.755	0.537	1																					
Sr	0.031	0.284	0.758	0.310	0.256	0.317	0.100	0.341	−0.106	1																				
Cd	−0.094	0.427	0.202	0.052	0.311	0.407	−0.013	−0.034	−0.095	0.469	1																			
Bi	0.764	0.497	0.834	0.874	0.627	0.435	0.693	0.769	0.379	0.400	0.030	1																		
V	0.911	0.666	0.244	0.455	0.378	0.248	0.926	0.718	0.739	−0.127	−0.113	0.581	1																	
Ca	0.037	0.222	0.768	0.277	0.198	0.238	0.115	0.378	−0.074	0.987	0.425	0.403	−0.132	1																
P	0.502	0.576	0.676	0.373	0.354	0.321	0.603	0.664	0.382	0.653	0.398	0.558	0.454	0.659	1															
Cr	0.866	0.395	0.430	0.751	0.510	0.365	0.753	0.669	0.426	−0.093	−0.161	0.684	0.777	−0.098	0.369	1														
Mg	0.516	0.287	0.856	0.950	0.671	0.537	0.381	0.557	−0.066	0.502	0.086	0.840	0.258	0.480	0.380	0.598	1													
Al	0.774	0.478	0.849	0.814	0.482	0.290	0.763	0.828	0.449	0.452	0.001	0.930	0.616	0.470	0.643	0.711	0.808	1												
K	0.493	0.253	0.951	0.866	0.575	0.437	0.399	0.633	−0.033	0.653	0.146	0.849	0.211	0.655	0.526	0.499	0.957	0.845	1											
Sc	0.808	0.534	0.270	0.487	0.272	0.120	0.856	0.605	0.799	−0.164	−0.186	0.592	0.864	−0.164	0.348	0.766	0.309	0.680	0.242	1										
Cs	0.597	0.301	0.937	0.880	0.593	0.414	0.511	0.695	0.097	0.565	0.109	0.913	0.329	0.578	0.540	0.576	0.938	0.901	0.982	0.366	1									
Nb	0.213	0.215	0.755	0.243	0.173	0.163	0.312	0.532	0.121	0.839	0.412	0.438	0.024	0.881	0.776	0.057	0.392	0.532	0.616	−0.014	0.596	1								
Rb	0.449	0.271	0.964	0.805	0.565	0.427	0.377	0.613	−0.002	0.718	0.194	0.855	0.180	0.726	0.584	0.417	0.911	0.829	0.982	0.202	0.968	0.684	1							
Sn	0.676	0.505	0.324	0.264	0.189	0.090	0.810	0.643	0.860	0.055	0.046	0.496	0.719	0.090	0.602	0.554	0.134	0.587	0.194	0.798	0.310	0.362	0.221	1						
Zr	0.577	0.413	0.012	−0.033	−0.137	−0.201	0.744	0.472	0.913	−0.191	−0.124	0.239	0.695	−0.151	0.261	0.351	−0.172	0.358	−0.128	0.776	0.003	0.069	−0.123	0.786	1					
Ce	0.582	0.821	0.264	0.328	0.462	0.412	0.640	0.376	−0.654	0.136	0.277	0.461	0.633	0.109	0.484	0.391	0.187	0.447	0.167	0.627	0.245	0.134	0.198	−0.637	−0.537	1				
In	0.571	0.242	0.021	0.103	−0.091	−0.244	0.644	0.355	0.793	−0.314	−0.326	0.296	0.630	−0.284	0.097	0.433	−0.036	0.415	−0.034	0.802	0.101	−0.067	−0.059	0.647	0.864	0.368	1			
Be	0.218	0.377	0.819	0.623	0.475	0.419	0.219	0.418	−0.068	0.831	0.263	0.657	0.076	0.794	0.548	0.189	0.770	0.652	0.810	0.092	0.746	0.576	0.849	−0.072	−0.211	0.224	−0.207	1		

	Mo	Pb	Zn	Ni	Co	Mn	Fe	As	Th	Sr	Cd	Bi	V	Ca	P	Cr	Mg	Al	K	Sc	Cs	Nb	Rb	Sn	Zr	Ce	In	Be	Li	Pd
Li	0.512	0.247	0.956	0.838	0.550	0.402	0.433	0.660	0.005	0.651	0.141	0.844	0.227	0.665	0.548	0.502	0.934	0.861	0.994	0.259	0.985	0.661	0.977	0.239	−0.076	0.170	0.013	0.781	1	
Pd	0.515	0.330	0.013	0.002	−0.120	−0.144	0.618	0.483	0.588	−0.147	−0.102	0.195	0.565	−0.118	0.076	0.245	−0.094	0.240	−0.072	0.542	0.014	−0.024	−0.089	0.448	0.738	0.348	0.548	−0.137	−0.049	1

Table 2.
Result of correlation analysis of selected elements.

	Component					
	1	2	3	4	5	6
Mg	0.959					
Ni	0.956					
Cs	0.921		0.343			
K	0.909		0.393			
Te	0.900					
Li	0.893		0.430			
Ti	0.881					
Rb	0.854		0.488			
Bi	0.850	0.376				
Al	0.812	0.481				
Zn	0.795		0.563			
Cu	0.770	0.354	0.319	0.315		
Tl	0.769		0.511			
U	0.734	0.351		0.379		
Cr	0.711	0.476				
Co	0.662			0.576		0.349
Na	0.632		0.358	0.358	−0.335	
Be	0.628		0.520	0.380		
Zr		0.969				
Hf		0.948				
Th		0.943				
Ga	0.420	0.864				
In		0.845				
Sc	0.388	0.841				
Sn		0.827				
Fe	0.428	0.826				
V	0.347	0.818				
Pd		0.735				
Mo	0.602	0.706				
Sb	−0.320	0.618			0.305	0.564
As	0.584	0.608	0.313			
Ce		0.603		0.542		
Se			0.942			
Nb	0.307		0.914			
Ca	0.311		0.903			
Sr	0.318		0.862			
P	0.350	0.367	0.629		0.361	
Ba	0.300			0.843		
Pb		0.518		0.754		

Component						
	1	2	3	4	5	6
Y				0.737	0.569	
Mn	0.483			0.663		0.443
La	0.342			0.620	0.511	
Cd			0.455	0.521	0.381	
Hg					0.838	
Ag					-0.575	
Au					-0.500	

Table 3.
Rotated component matrix.

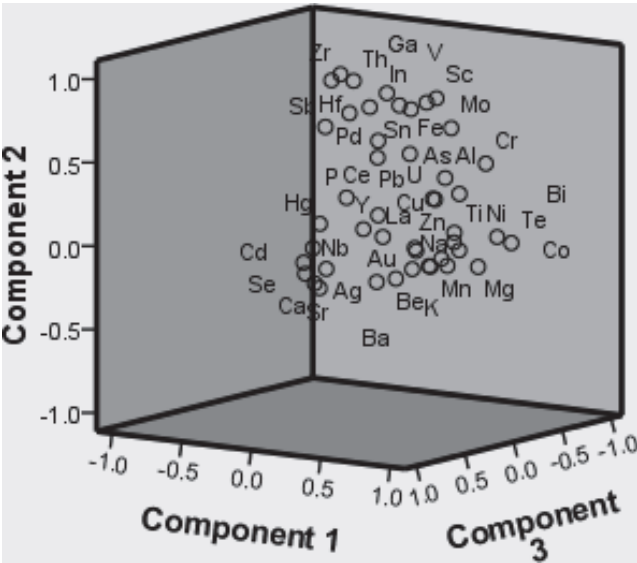


Figure 2.
3D component plot for soil factor analysis in rotated space.

were strongly related to mineralization. The presence of the country rock in the factor groups as accounted for by the principal component analysis decreases from factor 1 to factor 5. Factor 6 does not have the highest loading of any element but had the second highest loading of Mn, Sb and Co. This factor group was interpreted to imply the presence of minor or protore of Co-bearing manganite and also accounts for very strong leakages in the system during weathering of the rocks and ores in the area.

The depressions in the isograde plots were interpreted to be the zones of negative anomaly, while the positive anomalous zones were the peaks in the plots. The brown-coloured area defines the regional threshold, while the pinkish sky blue-coloured zones on the plots were interpreted as the local aureole. Deep blue zones were interpreted as the anomalous regions. The values of these zones were estimated from the corresponding values in the colour scale that is beside each plot.

From the plots, Ag had three positive anomalies that are defined by long. 4.13°E and lat. 11.125°N, long. 4.0°E and lat. 11.075°N and long. 3.35°E and 11.1°N, while its negative anomalies were defined by long. 4.09°E and lat. 11.07°N, long 4.05°E and lat. 11.07°N and long. 4.075°E and long. 11.09°N. Its regional threshold was ≤55 ppm, while the local aureole and anomaly had 70 ppm and >90 ppm, respectively. The positive anomalies of Au were defined by long. 11.225°E and lat. 4.0°N, while its negative anomaly was defined by long. 4.05°E and lat. 11.1°N. Its regional aureole

had ≤ 4 ppb, while its local aureole is 5.5 ppb. Its anomalous area had a concentration value of ≥ 6.5 ppb. Ba had its positive anomaly on the spot defined by long. 3.975°E and lat. 11.13°N . Its regional threshold had a concentration value of ≤ 150 ppm, while its local threshold and anomalous values were 230 ppm and ≥ 240 ppm, respectively.

Al had its positive anomaly defined by long. 4.05°E and lat. 11.09°N , while the negative anomaly was defined by long. 3.92°E and lat. 11.09°N . Its regional aureole, local aureole and anomalous value were ≤ 1.2 ppm, 1.5 ppm and > 1.6 ppm, respectively. As (Figure 3) had its positive anomalous zone defined by long. 4.05°E and lat. 11.1°N and long. 4.15°E and lat. 11.12°N . Its negative anomalies were defined by long. 4.075°E and lat. 11.075°N and long. 4.0°E and lat. 11.1°N . As had regional aureole, local aureole and anomaly with concentration values of ≤ 0.8 ppm, 1.0 ppm and ≥ 1.2 ppm, respectively.

The positive anomalous zone of Be was defined by long. 4.06°E and lat. 11.12°N (Figure 4). Its negative anomaly was defined by long. 4.1°E and lat. 11.11°N . The concentration of Ba described as regional threshold is ≤ 0.8 ppm and its local and anomalous concentrations were 1.2 ppm and ≥ 1.3 ppm, respectively. The positive anomaly of Bi is on long. 4.04°E and lat. 11.075°N , while long. 3.93°E and lat. 11.1°N define the negative anomaly (Figure 5). The regional threshold, local threshold and anomaly values were ≤ 0.13 ppm, 0.18 ppm and ≥ 0.21 ppm, respectively. Ca has its positive anomaly defined by long. 4.04°E and lat. 11.075°N , while its negative anomaly is defined by long. 4.05°E and lat. 11.06°N . The regional threshold value of Ca is ≤ 0.45 ppm while its local aureole and anomalous values were 0.6 ppm and ≥ 0.65 ppm. Cd positive anomaly was on the spot defined by long. 4.075°E and lat. 11.1°N . Its regional threshold, local threshold and anomalous values were ≤ 0.013 ppm, 0.017 and ≥ 0.019 ppm, respectively.

The positive anomaly of Co was defined by long. 4.04°E and lat. 11.05°N (Figure 6). Its negative anomaly was defined by long. 3.97°E and lat. 11.16°N , while its regional threshold, local aureole and anomalous values were ≤ 10 ppm, 14 ppm and ≥ 15 ppm, respectively. Cs has no negative anomaly but its positive anomalous point is defined by long. 4.04°E and lat. 11.06°N (Figure 7). Its regional threshold

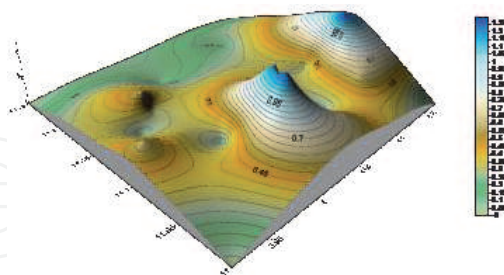


Figure 3.
3D isograde plot of As.

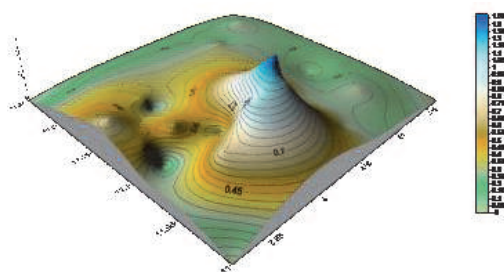


Figure 4.
3D isograde plot of Be.

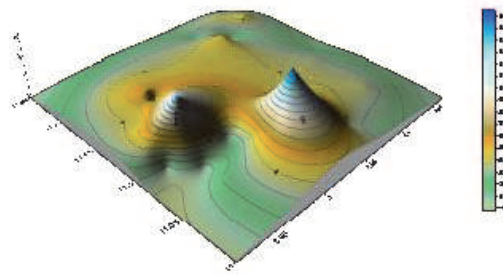


Figure 5.
 3D isograde plot of Bi.

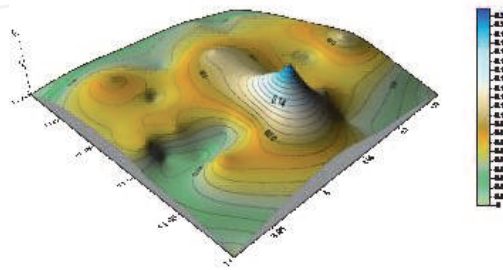


Figure 6.
 3D isograde plot of Co.

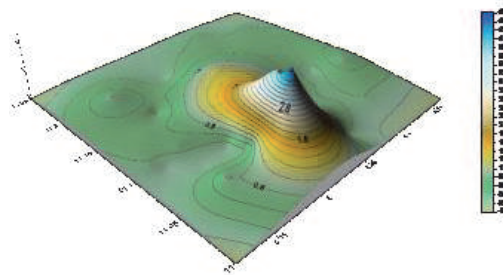


Figure 7.
 3D isograde plot of Cs.

value was ≤ 2.8 ppm, while its local threshold and anomalous values were 4 ppm and ≤ 4.2 ppm, respectively. The positive anomaly of K was on the spot defined by long. 4.04°E and lat. 11.07°N . Its regional threshold value was ≤ 0.3 ppm, while its local aureole and anomaly had values 0.44 ppm and ≥ 0.48 ppm, respectively. Li had its positive anomaly defined by long. 4.04°E and lat. 11.07°N . Its regional threshold, local aureole and anomalous values were ≤ 8 ppm, 26 ppm and ≥ 30 ppm, respectively. Mg also had its positive anomaly defined by lat. 11.07°N but long. 4.035°E , while its negative anomaly was defined by long. 4.06°E and lat. 11.025°N . Its regional threshold value, local aureole and anomaly had a concentration value of ≤ 0.012 ppm, 0.42 ppm and ≥ 0.48 ppm respectively. Mn had two positive anomalies that were defined by long. 3.36°E and lat. 11.12°N and long. 4.04°E and lat. 11.06°N (**Figure 8**). Its negative anomaly was defined by long. 4.07°E and lat. 11.05°E . Its regional threshold value, local aureole and anomalous values were ≤ 550 ppm, 800 ppm and ≥ 850 ppm, respectively.

The positive anomaly of Nb was on the spot defined by long. 4.04°E and lat. 11.075°N (**Figure 9**). Its negative anomaly was defined by long. 4.05°E and lat. 11.075°N . Its regional threshold value was ≤ 0.6 ppm, while the local aureole was 2.2 ppm. Its anomaly had a value of ≥ 2.5 ppm. Ni had its positive anomaly on long.

4.03°E and lat. 11.075°N (**Figure 10**). Its regional threshold value and local and anomalous values were ≤ 6 ppm, 22 ppm and ≥ 25 ppm, respectively. P had its positive and negative anomalies defined by long. 4.04°E and lat. 11.1°N and long. 4.1°E and lat. 11.125°N, respectively. Its regional threshold, local aureole and anomalous values were ≤ 0.005 ppm, 0.017 ppm and ≥ 0.019 ppm, respectively. Rb has long. 4.05°E and lat. 11.1°N defining its positive anomaly. Its regional threshold, local aureole and anomalous values are ≤ 13 ppm, 47 ppm and ≥ 55 ppm, respectively. The positive anomaly of Sr was defined by long. 4.03°E and lat. 11.075°N, while its negative anomaly was defined by long. 4.07°E and lat. 11.05°N. Its regional threshold, local aureole and anomalous values were ≤ 12 ppm, 44 ppm and ≥ 48 ppm, respectively. Zn had its positive anomaly on the spot defined by long. 4.05°E and lat. 11.1°N (**Figure 11**). Its regional threshold, local aureole and anomalous values were ≤ 12 ppm, 42 ppm and ≥ 48 ppm, respectively. Ce had three positive anomalies defined by long. 3.97°E and lat. 11.15°N, long. 4.075°E and lat. 11.05°N and long. 4.16°E and lat. 11.1°N (**Figure 12**). Its regional threshold and local aureole had a concentration value of ≤ 55 ppm and 75 ppm, respectively, while the anomalous concentration is ≥ 80 ppm. Similarly, Cr had its positive anomaly defined by the same longitude and latitude that defined that of Co, but its negative anomaly was

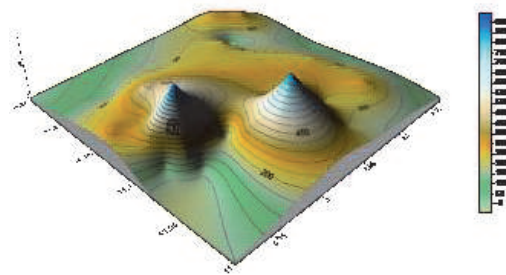


Figure 8.
3D isograde plot of Mn.

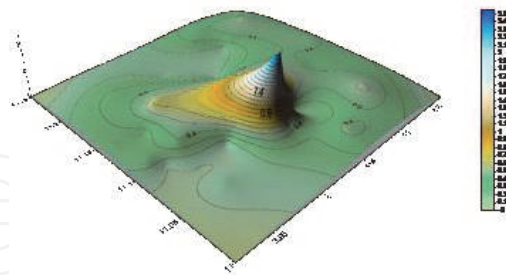


Figure 9.
3D isograde plot of Nb.

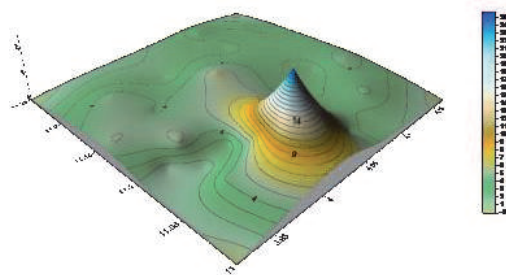


Figure 10.
3D isograde plot of Ni.

defined by long. 4.05°E and lat. 11.075°N (**Figure 13**). Its regional threshold value, local aureole and anomalous value were ≤ 28 ppm, 36 ppm and ≥ 40 ppm, respectively.

Fe had its highest concentration value on the spot defined by long. 4.16°E and lat. 11.1°N (**Figure 14**). Its regional threshold value was $\leq 2.4\%$, while its local aureole and anomalous values were 3.2% and $\geq 3.4\%$, respectively. The positive anomalies of Ga and Hf were defined by the same longitude and latitude that defined the anomalous point of Fe. The regional threshold, local aureole and anomalous value of Ga are ≤ 6 ppm, 8 ppm and ≥ 8.5 ppm, respectively, but the regional threshold value, local aureole and anomalous value of Hf were ≤ 0.22 ppm, 0.3 ppm and ≥ 0.32 ppm, respectively.

The positive anomaly of Hg was defined by long. 4.16°E and lat. 11.25°N, while its negative anomaly was defined by long. 4.1°E and lat. 11.1°N. Its regional threshold value was ≤ 22 ppm, while its local aureole and anomalous values were 26 ppm and ≥ 30 ppm, respectively. Like Fe, Ga and Hf, the positive anomaly of In was defined by long. 4.16°E and lat. 11.11°N (**Figure 15**). Its regional threshold value, local aureole and anomaly had values ≤ 0.03 ppm, 0.044 and ≥ 0.046 ppm, respectively. The positive anomaly of Mo was on the spot defined by long. 4.05°E and lat.

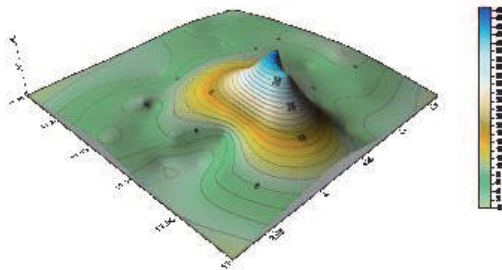


Figure 11.
3D isograde plot of Zn.

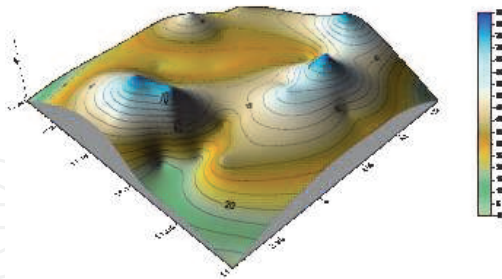


Figure 12.
3D isograde plot of Ce.

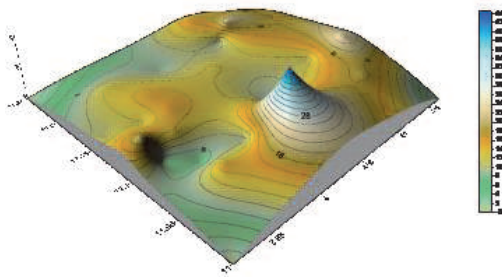


Figure 13.
3D isograde plot of Cr.

11.07°N (**Figure 16**). Its regional threshold had ≤ 0.25 ppm concentration, while its local aureole and anomalous value were 0.5 ppm and ≥ 0.9 ppm, respectively.

The positive anomaly of Pb is defined by long. 3.35°E and lat. 11.125°N. Its regional threshold, local threshold and anomalous values were ≤ 5 ppm, 17 ppm and ≥ 19 ppm, respectively. Pd anomaly was on the spot defined by long. 4.16°E and lat. 11.1°N (**Figure 17**). Its regional threshold value, local aureole and anomalous

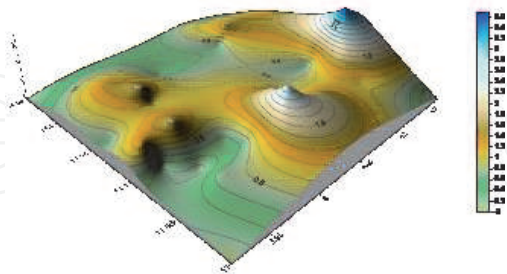


Figure 14.
3D isograde plot of Fe.

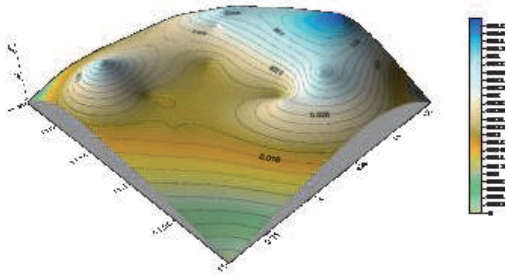


Figure 15.
3D isograde plot of In.

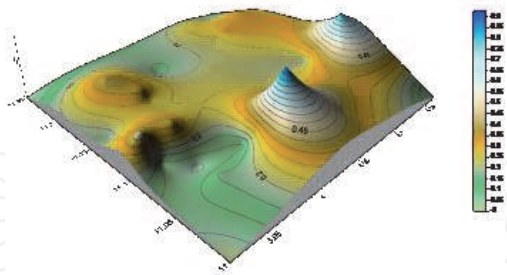


Figure 16.
3D isograde plot of Mo.

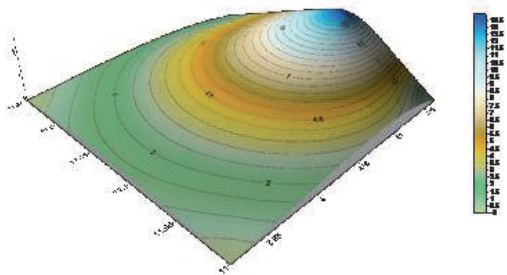


Figure 17.
3D isograde plot of Pd.

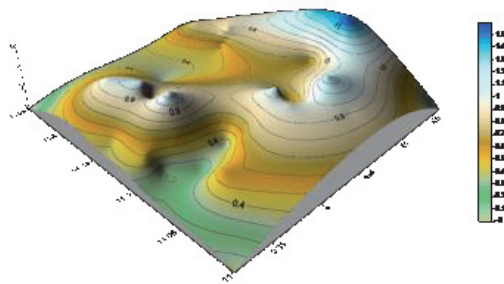


Figure 18.
 3D isograde plot of Sn.

concentrations are ≤ 3 ppm, 12.5 ppm and ≥ 13.5 ppm. Sb, Sc and Sn (**Figure 18**) all have their positive anomalies defined by long. 4.16°E and lat. 11.1°N . The negative anomaly of Sc was defined by long. 3.95°E and lat. 11.1°N , while its regional threshold value, local aureole and anomalous values were ≤ 2 ppm, 6.5 ppm and ≥ 7.5 ppm, respectively. The regional threshold value, local aureole and anomalous values for Sb were ≤ 0.015 ppm, 0.06 ppm and ≥ 0.065 ppm. The negative anomaly of Sn was defined by long. 4.05°E and lat. 11.075°N . Its regional threshold value, local threshold and anomalous values were ≤ 0.4 ppm, 1.3 ppm and ≥ 1.5 ppm, respectively.

The anomalous value of Th is on the spot defined by long. 4.16°E and lat. 11.09°N (**Figure 19**). Its regional threshold value was ≤ 3 ppm, while its local aureole and anomalous values are 12 ppm and ≥ 13.5 ppm, respectively. Long. 4.05°E and lat. 11.05°N define Ti positive anomaly. Its regional threshold, local aureole and anomalous values were ≤ 0.025 ppm, 0.08 ppm and ≥ 0.095 ppm, respectively. Tl positive anomaly was defined by long. 4.04°E and lat. 11.1°N . Its regional threshold value, local aureole and anomalous value were ≤ 0.08 ppm, 0.28 ppm and ≥ 0.32 ppm, respectively. U had its positive and negative anomalies defined by long. 4.05°E and lat. 11.05°N and long. 4.1°E and lat. 11.1°N . Its regional threshold value, local aureole and anomaly were ≤ 0.6 ppm, 2.1 ppm and ≥ 2.4 ppm, respectively.

Long. 4.16°E and lat. 11.1°N defined the positive anomaly of V (**Figure 20**), while its regional threshold, local aureole and anomalous values were ≤ 18 ppm, 60 ppm and ≥ 70 ppm, respectively. Y had its positive and negative anomaly defined by long. 3.92°E and lat. 11.17°N and long. 4.03°E and lat. 11.075°N . Its regional threshold, local aureole and anomalous values are ≤ 6 ppm, 22 ppm and ≥ 24 ppm, respectively. Long. 4.16°E and lat. 11.11°N defined the Zr positive anomaly (**Figure 21**). Its regional threshold, local aureole and anomalous values were ≤ 5 ppm, 17 ppm and ≥ 19 ppm, respectively. La had its positive anomaly defined by long. 3.98°E and lat. 11.15°N . Its regional threshold, local aureole and anomalous values were ≤ 18 ppm, 26 ppm and ≥ 28 ppm, respectively. Na had its own positive anomalies defined by long. 3.96°E and lat. 11.12°N and long. 4.05°E and lat. 11.1°N , while its regional threshold value is ≤ 0.0008 ppm. Its local and anomalous values were 0.0026 ppm and ≥ 0.0028 ppm. Te had its positive anomaly defined by long. 4.06°E and lat.

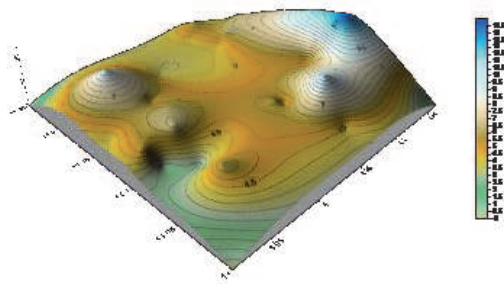


Figure 19.
 3D isograde plot of Th.

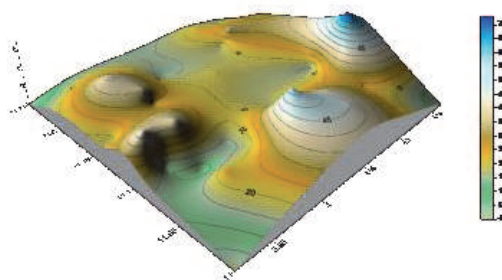


Figure 20.
3D isograde plot of V.

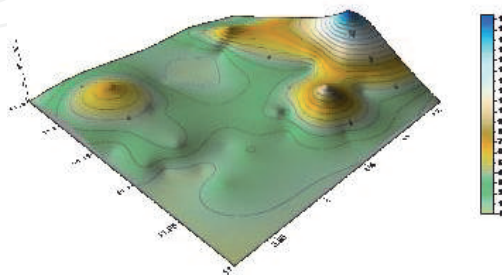


Figure 21.
3D isograde plot of Zr.

11.05°N. Its regional threshold value, local aureole and anomalous value were ≤ 0.012 ppm, 0.044 ppm and ≥ 0.048 ppm, respectively.

5. Discussion

Factor 1 of the soil factor analysis is predominated by the lithophile, chalcophile and siderophile elements. The distribution in this group is similar to the corresponding factor 1 in the ore factor analysis. In this factor group, most of the elements have mobilities which vary from low mobility to immobile [20]. Some of them, for example, Cu and Zn have varying mobilities between high to very low depending on the condition as against most of the elements that are immobile in the varying conditions. The association though related to weathered hydrothermal sulphide ore and sulphide-rich BIF is also aided by the mobility of the elements in fluctuating environmental conditions. The fluctuation in the condition is inferred from the inconsequential position occupied by the three types of elements that form the factor group. This scene is also repeated in factor 2 of the soil factor analysis. Most of the elements in this group are mainly transition metals. Their varying oxidation states coupled with the varying component of the materials that are coming together down the slope as the material is transported could account for the association in this group. At the beginning of this phase, the environmental condition favoured the lithophile element then followed by the condition that favoured the chalcophile. Midway into the phase, the condition became inconsistent before the condition that favoured the siderophile prevailed and capped by the chalcophile.

Factor 3 is typically of the lithophile elements with trapped single chalcophile element. The mobility of the chalcophile is similar to the mobility of the lithophile, thereby making it easy to be transported down the slope through the weathering path despite the differences in their chemical affinities and chemical properties. Factor 4 is also formed under relatively unstable environmental conditions that

fluctuated between the condition that favoured the siderophile, chalcophile and lithophile elements. The conditions that favoured the lithophile existed over a relatively long period especially towards the end of the phase and thereafter changed to the condition that favoured the chalcophile elements and then capped by the condition favouring siderophile. Factor 5 with Hg, Ag and Au is related to the weathered precious metals that were originally formed from hydrothermal sulphide ore [16]. Factor 6 with no highest loading of any element but has Co, Sb and Mn with fair loading implies the presence of minute Co-bearing manganese ore in the area.

Ag has three positive anomalies. These are in the eastern and southwestern parts of the study area. The local aureoles are aligned in NW-SE and NE-SW towards the southern part of Kaoje and its environs. Closely associated with these aureoles are negative anomalies that trend parallel to the positive anomalies. Al has its anomaly at long. 4.05°E and lat. 11.09°N. There are other positive anomalies in the NW (long. 3.95°E and lat. 11.2°N) and at the eastern end (long. 3.92°E and lat. 11.2°N). The negative anomaly of Al is well-defined at the western part of the mapped area (long. 3.92°E, lat. 11.09°N). These anomalies trend in NW-SE. Another spot of negative anomaly is to the right of the positive anomaly that extends from the southern part of the area towards the central part. As has its positive anomaly in almost the same place with Al. Though there are three peaks described as anomaly having the highest values, two of these peaks are twinned towards the centre of the area, while the third one is at the eastern end of the study area. The negative anomaly that is closely associated with the twinned anomalies towards the centre is also similarly positioned like the negative anomaly in Al. At the western end of this twinned peaks are two of each positive and negative anomalies. While the positives trend in NE-SW, the negative anomalies trend perpendicular to them in NW-SE direction.

Au has relative different distribution patterns from Ag, Al and As. Its negative anomaly is positioned where the three elements (Ag, Al and As) have their positive anomalies. This relationship in the position of the negative anomaly of Au indicates its depletion in the minerals formed or path-found by the three elements. Other peaks of anomaly of Au are in the SE corner and eastern and western parts of the area. These peaks like the negative anomalies are aligned in almost east-west direction with the exception of the peak in the northern part. The three positive anomaly peaks in Ba trend essentially in NW-SE with its highest concentration point defined by lat. 11.13°N and long. 3.975°E. This point of highest concentration of Ba corresponds to local aureole of elements like As, Al, Ag and Au. There is no negative anomaly except sharp decrease to the background value within the area of study. These slopes flank the peaks and also separate the peaks from each other.

Like As, Be has its anomaly in the southern part extending towards the central part of the study area. There are positive anomalies that are similarly positioned in the western half of the area except that while the positive anomalies in this half trend in NE-SW for As, those in Be trend in NW-SE. In like manner, the negative anomalies in Be trend in NE-SW, but those in As trend in NW-SE. Be also has a twin peak of anomaly like As, but one of it is not well-defined. Their distribution pattern is not identical but has similar position of their anomalies. Bi has a distribution pattern that is closely similar to that of As in terms of their positive and negative anomalies. Its anomalous point is defined by lat. 11.075°N and long. 4.04°E. These peaks slope towards the north. There are few negative anomalies that are evenly distributed in the four quadrants of the area studied. Ca has a point of positive anomaly towards the centre of the area. This area is defined by long. 4.05°E and lat. 11.1°N. The negative anomaly is poorly defined in the NE and SE parts of Kaoje and its environs.

Cd has ridge of anomaly that trend in NW-SE. The other anomaly is almost perpendicular to the broad NW-SE trending anomaly. Ce has its aureole in the western and SE part essentially. The extreme NE and SW part are relatively depleted in Ce. The Ce anomaly defines an arc curving back at the southern part. Cr has its anomaly at lat. 4.05°E and long. 11.075°N. Its negative anomalies trend in almost E-W direction. It shares some point of anomaly with elements like As and Bi. With the exception of slightly elevated concentration at the western part of the area (lat. 3.965° E and long. 11.120°N) essentially, the distribution of Co is almost identical with that of Cr. They (Cr and Co) have their anomaly in the same spot, while the distribution pattern of Cs and K is identical and similar with that of Ca. Their anomaly point is defined by lat. 4.05°E and long. 11.06°E. This anomaly trends in N-S direction. The anomaly of Ca does not cover larger area; the anomaly of Cs, K, Li and Mg covers relatively larger area compared with that of Ca, Bi and Cr. Their distribution pattern is also identical sharing the same point of anomalous concentration. There are passive zones of depletion which fall generally under regional threshold. Fe has its highest concentration in the eastern part of the study area and an anomaly that is described as local aureole in the southern part of the study area. These two peaks of anomalies are also observed in the isograde plot of As. With little variations, its distribution pattern is closely related to the distribution pattern of Cr and As.

Ga and Hf have different distribution patterns, but their zones of anomaly are similarly positioned in the eastern part of the area. This part is similarly shared by Fe, As and Cr essentially. While the negative anomaly in Ga trends in NW-SE direction essentially, the negative anomaly in Hf is randomly oriented. Hg has its peaks trending in NW-SE and at the extreme NE. This aureole is closely associated with negative anomaly that trends also in NW-SE. The anomaly at the extreme NE end is similarly positioned like the one in Cd, while the aligned NW-SE aureoles are similar to those in Cd. In is enriched in the eastern half of the study area. There is an aureole in the NW part, while the remaining area is relatively depleted in In. this depleted zone coincide with the boundary between the sedimentary rocks and the basement rock exposures. It zones of highest concentration are in the extreme eastern part where Fe, Cd, etc. also have theirs. No negative anomaly is seen as the values of depression are relatively higher than the values in the extreme NW and SW part of the area.

The distribution pattern of La is similar to that of Hg. Its point of highest aureole is defined by lat. 11.15°N and long. 3.98°E. The aureoles in La form a poorly defined curve shape that trends mainly in NW-SE direction. The extreme SE part is also slightly enriched in La but not as high as the central to NW part of the study area; the depleted zones flank the aureoles. Mn plot is identical with that of Co; it shares the same spot of anomalous concentration with Co and one of Cr anomalous concentration area. The aureole trends in NW-SE and decreases from the SW half towards the extreme NE part. Though not identical, other elements like Cs, K, Li, Mg, Ca, Bi, Cr, etc. have their anomalous point in either point of the anomalous concentration of Mn and Co. Like Mn, Mo has its highest point of concentration in the southern part of the area. There is also a relatively high concentration in the eastern part where Fe has one of its aureoles. Other slightly enriched zone of Mo is the western part. The positive aureole of Mo trends almost perpendicular to the positive aureole of Mn. With the exception of two well-defined peaks of aureoles, other patterns of distribution of these elements are alike.

Na has two peaks of positive anomaly. These peaks are located in the western and central parts of the area study. The western aureole is related to the western aureole of Mn though the Mn aureole is not as broad as that of Na but is more steep sided than that of Na. The area study is slightly more enriched in Na except the extreme four corners of the area. Nb has similar distribution pattern with Ca. The

study area is slightly more enriched in Nb relative to Ca, although they both have their positive aureole defined by the same latitude and longitude. The SW part of the area is more depleted in Nb, while the central part is enriched and trends perfectly in NW-SE direction. At the SE end of the positive anomaly, there is a zone of negative anomaly. This zone of Nb negative anomaly coincides with the zone of the most pronounced Au negative anomaly. Other elements with their positive anomaly or one of their positive anomalies defined by lat. 11.075°N and long. 4.05°E or closely related to that of Nb include Ca, Mg, K, Cs, Li, Be and As. Ni has its distribution pattern identical with that of Mg but the western part of the area is slightly depleted in Ni. The southern part of the study area is more enriched in Ni relative to the rest of the area. The aureole has >23 ppm concentration, while its local aureole has a concentration value of 21 ppm. Besides the fact that Li, Cs and K have primitive peaks closely associated with their aureoles, their distribution patterns and the distribution pattern of Ni are alike when their zones of anomaly are compared together. Ni also has its positive anomaly similarly positioned like the aureole of elements like Co, Bi and Al even though their distribution pattern is different. The positive aureole of Ni coincides with one of the positive aureoles in As while it is within the enriched zone of Be that trend NE-SW from the southern part. Au has its negative anomaly where Ni has its positive anomaly. This implies that Au depletion indicate the present of mineralization that is indicated by anomalous high concentration of Ni in this area.

Like Nb, P has its positive aureole defined by lat. 11.1°N and long. 4.05°E. The spot is shared or closely related to by the aureole of other elements like Li, Al, As, Be, Ca, Cs, K, etc. Its distribution pattern is similar to the distribution pattern of Mo, La, Hg, Ga, Fe and Ce essentially. Though with relatively lower concentration values and in rare cases slightly high concentration, the zones of positive enrichment and depletion of these elements are closely related. Cr has relatively high enrichment in all the areas where P also has its high enrichment but the zone of P depletion in the eastern part is not seen in Cr isograde plot. Pb has its highest concentration (>19 ppm) in the western part of the area defined by long. 3.35°E and lat. 11.125°N. Like P, La, Fe, Ce, etc., its distribution pattern forms a poorly defined U-shape. The zone of its highest positive anomaly has negative anomalies closely associated with it in the SW and NE parts. Other peaks of positive anomalies are in the southern and extreme eastern parts of the area. Its zone of highest concentration is related to the zone of highest concentration of elements like La, Ce, Cd and Ba. The peaks of positive anomaly in the western and southern parts relate very well with the two peaks of positive anomaly in Mn, while the peaks of positive anomaly of Pb in the southern and eastern parts are closely associated with the peaks of highest Fe concentration. Fe also has slightly elevated value in the western part where Pb has its highest concentration value. Other elements have their positive anomalies in one or more zone of Pb enrichment even though their distribution patterns are not the same.

Pd has its aureole in the western end of the study area. Its concentration decreases gradually towards the western end of the area. The zones of its highest concentration in the eastern part of the area coincide perfectly with one of the positive aureoles of Fe, Mo, In, Ga, Hf, etc. The Rb style of distribution is identical with the distribution pattern of Li, K and Cs. Its zone of highest concentration is wholly or partly shared besides the aforementioned elements by Al, As, Be, Bi, Ca, Cd, Co, Mg, Mn, Mo, Nb, Ni, P, etc. The peaks of its aureoles trend essentially in NE-SW direction. The negative anomalies are not well-defined but are closely associated with positive anomaly in the eastern part of the area.

Sb has its zones of highest concentration in the extreme eastern and western end of the area. Other zones of enrichment are closely associated with these two peaks

defining a slightly different NE-SW trending direction. The distribution pattern is relatively unique, but its zone of highest concentration in the eastern end is related to the zones of highest concentration of Fe, Mo, In, Ga and Hf. The extreme NW and SW are the most depleted zones of Sb. Other areas have slightly elevated value relative to other elements.

With the exception of break in the ridge of positive anomaly of Sc in the western part of the area, the distribution pattern of Sc and Sn is identical. They both have a ridge of positive anomaly that rises in the NW going through the southern part and turning through the eastern part to end in the NE part of the area study. They have two peaks of positive aureoles. One of the aureoles is situated in the eastern part where elements like Fe, Mo, In, Ga and Hf have their or one of their positive anomalies. The second positive aureole of Sc is in the southern part of the area, while that of Sn shifts slightly to the SE part of the area. They have their negative anomalies trending essentially NW-SE in the western end and NE-SW in the eastern end. Sr has slight enrichment in the western part. These enrichments trend in NW-SE terminating in the central part. Its zone of highest concentration is in the centre. This centre where it has its highest concentration is defined by long. 4.05°E and lat. 11.075°N. Its zone of highest concentration is similarly shared by Rb, Al, As, Be, Bi, Ca, Cd, Co, Mg, Mn, Mo, Nb, Ni, P, etc. Its distribution pattern is identical with the distribution pattern of Ca.

The distribution pattern of Te is similar to the distribution pattern of Na. Its peak (positive anomaly) is in the central to SE part of the area. Its anomaly trends in NW-SE but generally decreases to the background value of ≤ 0.028 ppm. Th has its highest concentration in the eastern part. Other area with relatively high concentration of Th is in the SE and is closely associated with the zone of Th positive anomaly. The concentration of Th in the western half is also relatively high but not as high as the concentration in the eastern part. The western aureole trends in N-S direction with about three alternations in its concentration with about three alternations in its concentration. The extreme NW and SW corners of the area are relatively the most depleted zone for Th. The position of the positive anomaly of Th is the same with the position of positive anomaly of Fe, Sn, Sc, Sb, Pd, In, Hf and As. Mo and Ce has one of their positive anomaly in this eastern part, but the zone of highest concentration of Ag is just slightly off the zone of Th highest concentration to the west.

Ti, Tl and U have their positive anomalies defined by lat. 11.075°N and long. 4.04°E and lat. 11.08°N and long. 4.04°E and lat. 11.07°N and long. 4.04°E, respectively. Though with slight variation, these elements have their positive anomalies where elements like Sr, Rb, Ni, P, Nb, Li, K, Cs, Co, Cd, Ca, Bi, Be, As and Al have theirs or one of their positive anomalies. This zone is also though not exactly but similarly positioned like one of the Mn positive anomaly. Ti and Tl have their highest concentration within the central part of the area. Ti concentration is slightly high in the eastern and extreme NE part, but Tl has its own concentration decreasing gradually towards the extreme west, thereby making the western half slightly more enriched than the eastern half. Both Ti and Tl have sharp depression to the background value. These depressions are similarly oriented in poorly defined NWW-SEE in the western half of the area. Unlike Ti and Tl, U has its concentration in the central part which forms a ridge of positive anomaly extending from the central area to the NW of the area where it forms a twin peak. The peak to the east among these two peaks has slightly higher concentration than that in the western part. There are negative anomalies in the western half and eastern part of the area. The negative anomalies in the western half that are well-defined trend in NE-SW. The poorly defined negative anomaly trends with one of the well-defined in NW-SE. The U negative anomalies in the eastern half of the area trend mainly in NE-SW.

The distribution pattern of V is similar to the distribution pattern of Th, Sc, Sn, Pb, P, Mo, La, Hg, Ga, Fe, Cr and Ce. Its zone of highest concentration (>65 ppm) is in the extreme eastern part, while it is also enriched in the southern part. These two zones of highest concentration are similar to the zone of highest concentration of Fe, Sc and Mo. The enrichment in the western half is almost identical with that of Fe when the position of the zones of highest enrichment and depletion are compared. The central part of the area is the most depleted zone of V. Like some other elements, e.g. Hf, its distribution pattern has poorly defined U-shape. The zone of highest concentration of Y (>23 ppm) is in the NW part of the area. This area is flanked by negative anomaly in the SW and NE part. The zone of relative high concentration of the anomaly, usually ≥ 16 ppm, is restricted to the western half of the study area and trends in NW-SE direction. The extreme SW and SE corner is relatively depleted of Y (≤ 5 ppm), while other areas have elevated value that range between 5 and 16 ppm. The positive anomalous zone of Y is similarly enriched in Pb, La, Hg, Cd, Ce, Ba and Mn.

The distribution pattern of Zn is identical with the distribution pattern of Rb and almost identical with the distribution pattern of Li, K and Cs. Both Zn and Rb have two peaks at the crest of their anomalous zone in the central part of the study area. The peak in the northern part out of these two peaks is slightly more prominent than the one in the south. These two peaks are also present in the same position in the isograde plot of Tl despite the fact that its style of distribution is slightly different from that of Zn and Rb. Other similarities in the distribution pattern of Zn and Rb include the twin slightly enriched area in the NW part of the area and also the negative anomaly in their isograde plot. Other elements that have their positive anomaly where Zn has its own and with similar distribution pattern include Ti, Mg, Cs, etc. Cs and K have the two peaks, but their peak in the southern part is more prominent than the one in the northern part. The zone of Zn anomaly is shared by the anomaly of Al, As, Be, Bi, Ca, Cd, Co, Mn, Nb, P and Ni essentially. Zr highest concentration is ≥ 19 ppm. This concentration is in the eastern part of the area. With the exception of elevated value (≤ 9 ppm) in the NW part of the area, the enrichment of Zr is restricted to the eastern half of the area especially where Fe, Th and Pd have their highest concentration.

6. Conclusion

From integrated field observation, geochemical study, statistical analysis and isograde plottings, it was concluded that the area investigated is mineralized with goethite and manganite ores, while there are minor enrichments of tourmaline and silicate minerals like chalcedony. It was also concluded that the eastern and southern parts of the study area is mineralized with goethite, while the western and southern parts are mineralized with manganite. Furthermore, in exploring for iron-manganite mineralization in this area, manganite has as its pathfinder the following associations $\text{Zn} + \text{As} + \text{Be} + \text{Bi} + \text{Co} + \text{Nb} + \text{Ni} + \text{Cs} \pm \text{P} + \text{Al} + \text{Ca} + \text{Cd} + \text{Rb} + \text{Li} + \text{K}$, while $\text{Zr} + \text{Th} + \text{Pd} + \text{Mo} + \text{V} + \text{Sn} + \text{Cr} + \text{Ce} + \text{In} \pm \text{Sc} + \text{P} + \text{Pb}$ associations are related to iron mineralization.

IntechOpen


IntechOpen

Author details

Olufemi Sijuade Bamigboye
Department of Geology and Mineral Sciences, Kwara State University, Malete,
Nigeria

*Address all correspondence to: olufemi.bamigboye@kwasu.edu.ng

IntechOpen

© 2020 The Author(s). Licensee IntechOpen. This chapter is distributed under the terms of the Creative Commons Attribution License (<http://creativecommons.org/licenses/by/3.0>), which permits unrestricted use, distribution, and reproduction in any medium, provided the original work is properly cited. 

References

- [1] Fabris AJ, Keeling JL, Fidler RW. Soil geochemistry as an exploration tool in areas of thick transported cover, Curnamona Province. *MESA Journal*. 2009;**54**:32-40
- [2] Martin AP, Turnbull RE, Rattenbury MS, Cohen DR, Hoogewerff J, Rogers KM, et al. The regional geochemical baseline soil survey of southern New Zealand: Design and initial interpretation. *Journal of Geochemical Exploration*. 2016;**167**: 70-82
- [3] Omorinoye OA, Adekeye JID. Soil geochemical survey of eruku and environs. *Journal of Environment and Earth Science*. 2013;**3**(7):105-115
- [4] Filgueiras AV, Lavilla I, Bendicho C. Evaluation of distribution, mobility and binding behavior of heavy metals in surficial sediments of Louro River (Galicia, Spain) using chemometric analysis: A case study. *Science of the Total Environment*. 2004;**330**:115-129
- [5] Bowen HJM. *Environmental Chemistry of the Elements*. London: Academic Press; 1979. pp. 333
- [6] David RH. An Assessment of Soil Geochemical Methods for Detecting Copper-Gold Porphyry Mineralization through Quaternary Glaciofluvial Sediments at the WBX-MBX and 66 Zones, Mt. Geoscience BC Report. North-Central British Columbia: Milligan; 2010. p. 75
- [7] Akilolu F. Exploration and Resource Estimation of the Manganese Deposit in Kaoje, Kebbi State. *NGSA Report*. 2007. p. 70
- [8] Bamigboye OS, Adekeye JID, Kadioglu YK, Adedoyin AD, Omorinoye OA. Geochemistry and origin of Fe-Mn oxide mineralization in Kaoje-Derena and their environs, Northwestern Nigeria. *Arabian Journal of Geosciences*. 2018;**11**:570-587
- [9] Adekoya JA. The geology and geochemistry of the Maru banded iron formation, Northwestern Nigeria. *Journal of African Earth Sciences*. 1998; **27**(2):241-257
- [10] Mucke A. The Nigerian manganese-rich iron-formations and their host rocks from sedimentation to metamorphism. *Journal of African Earth Sciences*. 2005;**41**(5):407-436
- [11] Okorie IM, Ayoade EO, Okunola OW, Okunlola OA. Manganese Mineralization in Parts of Northwestern Nigeria. In: *Book of Abstract, 45th NMGS Annual International Conferences*; Owerri, Nigeria. 2009
- [12] Okorie IM, Ayoade EO, Okunola OW, Okunlola OA. Geological setting and occurrences of copper mineralization around Talata Mafara and Anka Areas, Northwestern Nigeria. In: *Book of Abstract, 45th NMGS Annual International Conferences*; Owerri, Nigeria. 2009
- [13] Fillie S. Genesis and paragenesis of the tetravalent Mn ores and Mn-Fe ores in secondary banded iron formations from Nigeria. In: *Proceedings of the 3rd World Conference on Applied Sciences, Engineering and Technology*, Kathmandu, Nepal. 2014. pp. 318-328
- [14] Fillie S. Chemical mineralogy of supergene ores in banded iron formations from Northern and South-Central Nigeria. In: *Proceedings of the 3rd World Conference on Applied Sciences, Engineering and Technology*, Kathmandu, Nepal. 2014. pp. 329-339
- [15] Vareikiene O, Lehtonene M. Heavy minerals study of soils: Techniques, their limitations and advantages. *Geologija*. 2004;**46**:1-7

- [16] Levinson AA. Introduction to Exploration Geochemistry. Wilmete, USA: Applied Publishing Ltd; 1981. p. 613
- [17] McQueen KG. Element fractionation and mineral hosts in the regolith. In: Book of Abstracts—LEME AMEC Minerals Exploration Seminar. 2004. pp. 19-23
- [18] Dempster M, Cooper MR, Dunlop P, Scheib AJ. Using soil geochemistry to investigate gold and base metal distribution and dispersal in the glaciated North of Ireland. In: Young ME, editor. Unearthed: Impacts of the Tellus Surveys of the North of Ireland. Dublin: Royal Irish Academy; 2016. DOI: 10.3318/978-1-908996-88-6. ch7
- [19] Tsikos H. Petrographic and geochemical constraints on the origin and post-depositional history of the hotazel iron-manganese deposits, kalahari manganese field, South Africa [Ph.D. thesis]. Rhodes University; 1999. p. 217
- [20] Andrew-Jones DA. The Application of Geochemical Techniques to Mineral Exploration. Vol. 11(6). Golden/Colorado: Colorado School of Mines. Mineral Industries Bulletin; 1968. pp. 1-31